MELTING PROCESS MODELLING OF CARREAU NON-NEWTONIAN PHASE CHANGE MATERIAL IN DUAL POROUS VERTICAL CONCENTRIC CYLINDERS

by

Mohsen TALEBZADEGAN[a], Mojtaba MORAVEJ[a,b*], Ehsanolah ASSAREH[a], and Mohsen IZADI[c]

[a] Department of Mechanical Engineering, Dezful Branch, Islamic Azad University, Dezful, Iran
[b] Department of Mechanical Engineering, Payame Noor University, Iran
[c] Mechanical Engineering Department, Faculty of Engineering, Lorestan University, Khorramabad, Iran

Original scientific paper
https://doi.org/10.2298/TSCI200711329T

In this paper a numerical simulation of the melting process of Carreau non-Newtonian phase change material inside two porous vertical concentric cylinders included constant temperatures of the inner and outer walls, represented by T_h and T_c, respectively. Half of the void between the two pipes is filled with copper porous media and paraffin wax as a phase change material. The governing equations are converted into a dimensionless form and are solved using the finite element method. The enthalpy porosity theory is applied to simulate the phase change of phase change material while the porous media follow to the Darcy law. Outcomes are shown and compared in terms of the streamline, isotherm, melting fraction and mean Nusselt numbers. The solid liquid interface location and the temperature distribution are predicted to describe the melting process. The effects of the Carreau index, porosity and non-dimensional parameters such as Stefan number, Darcy number, and Rayleigh number are analyzed. Our results indicate a good agreement between this study and the previous investigations. The results show that an increase in Rayleigh number, Stefan number, and Darcy number, increases the melting volume fraction and reduces the melting time. Also, the time of melting non-Newtonian phase change material decreases when Carreau index and porosity decrease.

Key words*: phase change materials, porous media, heat transfer enhancement, non-Newtonian fluid, natural convection*

Introduction

The study of solid-liquid PCM in porous media has received a lot of attention in recent years because of its vital role in industrial applications, such as solar power collectors, electronics devices, building, computer sciences and heat exchangers [1]. According to this concept that a small segment of PCM can store a considerable amount of energy during of phase change process. The thermal storage technology is important in the energy saving performance. Liu *et al.* [2] a numerical model is established to predict the phase PCM melting process in porous media. The heat transfer enhancement technique using metal foam in a shell-and-tube

* Corresponding author, e-mail: moravej60@pnu.ac.ir

type latent heat thermal energy storage unit is investigated. The solid liquid phase change phenomenon is solved with enthalpy porosity theory. Their results show that the phase change heat transfer can be enhanced by more than seven times than the pure PCM. In this research, analysis was performed using the PCM of paraffin wax RT58 and the metal matrix of copper. Chamkha *et al.* [3] The melting process of a nanoPCM is researched in square cavity with a high temperature cylinder inserted in the middle of the cavity in the existence of both single and hybrid nanoparticles. The impacts of the amount of nanoparticles, the Fourier number, the thermal conductivity parameter, and the viscosity parameters are investigated. They found that the melting rate is much larger when the Fourier number changes in the middle of 0-0.5. Tian and Zhao [4], experimented the effects of copper foam on heat transfer enhancement on the melting process of paraffin wax RT58. The main finding of their research is that the heat conduction rate is increased significantly by using metal foams. They found that by adding the metal foam, PCM heat transfer performance is enhanced. Also, their results showed that the metal foams with smaller porosity could have a better heat transfer efficiency as compared to those with larger porosity.

Nowadays, non-Newtonian fluid-flow in porous media appears in different fields of engineering application, such as oil recovery, foods [5] and material processing. Non-Newtonian fluids in porous media shows a non-linear behavior than the Newtonian one. The non-Newtonian fluids in natural-convection filled with pure fluid have been investigated [6-16] in some studies. Harab *et al*. [17], numerically investigated 2-D time-dependent natural-convection heat transfer of a non-Newtonian nanofluid in the inside the two horizontal cylinders. The finite volume method was utilized in the research. From conclusions it can be inferred that with by adding to the power law index from 0.6-1.4, the heat transfer decreases with a rate of about 78%. Mehrian *et al.* [18] examined the theory of using non-Newtonian phase change nanomaterial of the power-law model to increase cooling in the space between two vertical insulated cylinders. The Galerkin method was used to analyze the governing equations. Moreover, the moving mesh method was used to model the melting process. The results showed that the addition of nanoparticles to the PCM reduces the melting speed as well as the Nusselt number. Ghalambaz *et al.* [19] studied the theory of the effect of the presence of nanoparticles of mesoporous silica on heat transfer in the melting process of non-Newtonian octadecane PCM in a square chamber. The moving mesh method was used to model the melting process. The results showed that the addition of mesoporous silica reduces the heat transfer. By adding 5% of the nanoparticles to the octadecane PCM, the heat transfer rate is reduced by up to 50%. In addition, the angle of the chamber plays an important role in the heat transfer rate so that at an angle of –75°, the heat transfer rate is reduced by up to 80%. Hashim *et al.* [20] presented a new modified Buongiornos model to study the flow of a non-Newtonian nanofluid belonging to the carreau model, which creates by wedge-shaped geometry. Besides, the characteristics of mass transport and heat transfer were also shown under the diffusion of the non-linear heat radiations. At first, the flow and heat equations were acquired dimensionlessly. Then, the set of the non-linear ODE were solved with the help of MATLAB software.

Model explanation

Figures 1(a) and 1(b) depicts a physical model in 2-D and 3-D views. As seen, the model is included two coaxial pipes with r_i, r_o, and L as inner and outer radius and height of the model, respectively. There has been a constant temperature difference between inner and outer pipes. The temperature of the inner pipe is higher than the outer pipe

($T_h > T_c$). Moreover, annulus surfaces above and below of the model have been considered to be thermal insulated. Copper foam as a high conductive porous medium, has covered on the left half of the space. The void space of the porous media and simple media on the half right has been filled by paraffin wax as PCM. Paraffin wax in the melting state is incompressible, non-Newtonian and flows in the laminar regime. Viscous dissipation, density variation (by phase change) in the domain and ever fluid, slip on the boundaries are negligible. The Boussinesq approximation is also valid for the melting PCM. Local thermal equilibrium conditions between the solid matrix of the copper foam and paraffin wax are dominant. It is worth noting that the thickness of both pipes is ignored. The thermophysical specifications of paraffin wax and copper foam are shown in tab. 1.

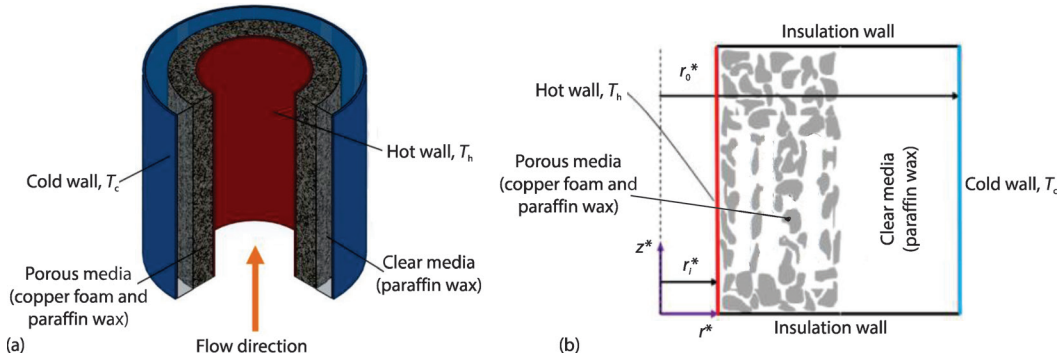

Figure 1. Axisymmetric schematic diagram of geometric model; (a) 3-D view and (b) 2-D view

Table 1. Specification of paraffin wax and copper foam [4]

	PCM (paraffin wax RT58)	Porous medium (copper foam)
Density of solid PCM, ρ_s [Kgm^{-3}]	880	8960
Density of fluid PCM, ρ_f [Kgm^{-3}]	76	–
Volumetric expansion coefficient, β [K^{-1}]	$6 \cdot 10^{-4}$	–
Melting temperature, T_f [K]	318-324	–
Thermal conductivity, K [Wm^{-1}K^{-1}]	0.2	401
Latent heat of fusion, L_f [kJkg^{-1}]	168	–
Specific heat in constant pressure, C_p [Jkg^{-1}K^{-1}]	2000	381

Governing equations

To simulate the melting and solidification process of non-Newtonian paraffin wax in double pipe space, the enthalpy porosity method has been employed. Brinkman-Darcy model is also used for the half porous media on the left. The non-dimensional form of governing equations for unsteady natural convection heat transfer of paraffin wax in copper foam and simple media considering the melting and solidification process in the form of continuity, momentum and energy equations are ritten [2, 4]:

$$\frac{1}{r}\frac{\partial(ru)}{\partial z}+\frac{\partial w}{\partial z} \tag{1}$$

Continuity equation:

– Momentum equation in *r*-direction

$$\frac{\rho_{\mathrm{PCM}}}{\varepsilon}\frac{\partial u}{\partial Fo}+\frac{\rho_{\mathrm{PCM}}}{\varepsilon^2}\left(u\frac{\partial u}{\partial r}+w\frac{\partial u}{\partial z}\right)=$$
$$=-\frac{\partial P}{\partial r}+\frac{\mathrm{Pr}}{\varepsilon}\left(\frac{\partial\left(\left(1+A_m\left(1-\varphi(\theta)\right)\right)\left[1+\left(\lambda\dot{\gamma}\right)^2\right]^{\frac{n-1}{2}}\right)}{\partial r}+\frac{\partial\left(\left(1+A_m\left(1-\varphi(\theta)\right)\right)\left[1+\left(\lambda\dot{\gamma}\right)^2\right]^{\frac{n-1}{2}}\right)}{\partial z}\right)\cdot$$
$$\cdot\left(\frac{1}{r}\frac{\partial}{\partial r}\left(r\frac{\partial u}{\partial r}\right)-\frac{u}{r^2}+\frac{\partial^2 u}{\partial z^2}\right)-\frac{\mathrm{Pr}}{\mathrm{Da}}\left(\left(1+A_m\left(1-\varphi(\theta)\right)\right)\left[1+\left(\lambda\dot{\gamma}\right)^2\right]\right)^{\frac{n-1}{2}}u+s(\theta)u \tag{2}$$

– Momentum equation in *z*-direction

$$\frac{\rho_{\mathrm{PCM}}}{\varepsilon}\frac{\partial w}{\partial Fo}+\frac{\rho_{\mathrm{PCM}}}{\varepsilon^2}+\left(u\frac{\partial w}{\partial r}+w\frac{\partial w}{\partial z}\right)=$$
$$=-\frac{\partial P}{\partial z}+\frac{\mathrm{Pr}}{\varepsilon}\left(\frac{\partial\left(\left(1+A_m\left(1-\varphi(\theta)\right)\right)\left[1+\left(\lambda\dot{\gamma}\right)^2\right]^{\frac{n-1}{2}}\right)}{\partial r}+\frac{\partial\left(\left(1+A_m\left(1-\varphi(\theta)\right)\right)\left[1+\left(\lambda\dot{\gamma}\right)^2\right]^{\frac{n-1}{2}}\right)}{\partial z}\right)\cdot$$
$$\cdot\left(\frac{1}{r}\frac{\partial}{\partial r}\left(r\frac{\partial w}{\partial r}\right)+\frac{\partial^2 w}{\partial z^2}\right)-\frac{\mathrm{Pr}}{\mathrm{Da}}\left(\left(1+A_m\left(1-\varphi(\theta)\right)\right)\left[1+\left(\lambda\dot{\gamma}\right)^2\right]^{\frac{n-1}{2}}\right)w+s(\theta)w+\mathrm{Ra}\,\mathrm{Pr}\,\theta \tag{3}$$

– Energy equation

$$\frac{\partial\theta}{\partial Fo}+\frac{\left(\rho C_p\right)_{\mathrm{PCM}}}{\left(\rho C_p\right)_{\mathrm{eff}}}+\left(u\frac{\partial\theta}{\partial r}+w\frac{\partial\theta}{\partial z}\right)+\varepsilon\frac{\left(\rho C_p\right)_{\mathrm{PCM}}}{\left(\rho C_p\right)_{\mathrm{eff}}}\frac{1}{\mathrm{Ste}}\frac{\partial\varphi(\theta)}{\partial Fo}=\frac{\alpha_{\mathrm{eff}}}{\alpha_{\mathrm{PCM}}}\left[\frac{1}{r}\frac{\partial}{\partial r}\left(\frac{\partial\theta}{\partial r}\right)+\frac{\partial^2\theta}{\partial z^2}\right] \tag{4}$$

where:

$$\left(\rho C_p\right)_{\mathrm{eff}}=(1-\varepsilon)(\rho C_p)_{\mathrm{porous}}+\varepsilon\left(\rho C_p\right)_{\mathrm{PCM}}$$
$$k_{\mathrm{eff}}=\left(1-\varepsilon\right)k_{\mathrm{porous}}+\varepsilon k_{\mathrm{PCM}}\qquad,\ \varphi(\theta)=\begin{cases}0 & \theta<0\\ \dfrac{\theta}{\Delta\theta} & 0<\theta<\Delta\theta\\ 1 & \theta>\Delta\theta\end{cases} \tag{5}$$
$$\alpha_{\mathrm{eff}}=\left(1-\varepsilon\right)\alpha_{\mathrm{porous}}+\varepsilon\alpha_{\mathrm{PCM}}$$

The non-dimensional variables are:

$$\mathrm{Pr}=\frac{\upsilon_{\mathrm{PCM}}}{\alpha_{\mathrm{PCM}}},\ \mathrm{Ra}=\frac{\mathrm{g}\beta_{\mathrm{PCM}}\Delta T(r_o-r_i)^3}{\upsilon_{\mathrm{PCM}}\alpha_{\mathrm{PCM}}},\ \mathrm{Ste}=\frac{C_{p\mathrm{PCM}}(T_{\mathrm{h}}-T_f)}{L_{\mathrm{f}}},\ \mathrm{Da}=\frac{k}{(r_o-r_i)^2}$$
$$r=\frac{r^*}{(r_o-r_i)},\ z=\frac{z^*}{(r_o-r_i)},\ u=\frac{u^*(r_o-r_i)}{\alpha},\ w=\frac{w^*(r_o-r_i)}{\alpha},\ \theta=\frac{T-T_f}{T_{\mathrm{h}}-T_f} \tag{6}$$
$$Fo=\frac{t\alpha}{(r_o-r_i)^2},\ p=\frac{p^*(r_o-r_i)^2}{\rho\alpha^2},\ \dot{\gamma}=\frac{\gamma^*(r_o-r_i)^2}{\alpha},\ \lambda=\frac{\lambda^*\alpha}{(r_o-r_i)^2},\ s(\theta)=-A_m\frac{1-\varphi(\theta)}{\left[\varphi(\theta)\right]^3+\varepsilon_p}$$

Here Pr, Da, Ra, Ste, $\varphi(\theta)$, $(\rho C_p)_{\text{eff}}$, k_{eff}, and α_{eff}, are Prandtl, Darcy, Rayleigh, and Stefan numbers, melting fraction, effective specific heat in constant pressure, effective thermal conductivity, and effective thermal diffusivity coefficient, respectively.

Dynamic viscosity for Carreau non-Newtonian melting PCM (under melting conditions) can be written [21]:

$$\mu(\dot{\gamma}) = \mu(\varphi)\left[1+(\lambda\dot{\gamma})^2\right]^{\frac{n-1}{2}},\ \ \mu(\varphi) = \mu_{\text{PCM}}\left(1+A_m(1-\varphi(\theta))\right) \tag{7}$$

The digression of Carreau index from unity depicts the degree of digression from Newtonian behavior that is $n < 1$ for pseudo-plastic, $n = 1$ for Newtonian, and $n > 1$ for dilatant fluids. Pseudo-plastic fluids are delineated by an apparent viscosity which descents with ascending shear rate, however in dilatant fluids the apparent viscosity increments with ascending shear rate.

The initial and boundary conditions are also changed in to the non-dimensional form:

$$\begin{gathered}
u(r,z,0)=0,\ \ w(r,z,0)=0 \ \text{ and } \ \theta(r,z,0)=\theta_{\text{int}} \\
u\left(r_i,z,Fo\right)=0,\ \ w\left(r_i,z,Fo\right)=0 \ \text{ and } \ \theta\left(r_i\ ,z\ \ ,Fo\right)=1 \\
u\left(r_o,z,Fo\right)=0,\ \ w\left(r_o,z,Fo\right)=0 \ \text{ and } \ \theta\left(r_o,z,Fo\right)=0 \\
u\left(r_i\le r\le r_o,0,Fo\right)=0,\ \ w\left(r_i\le r\le r_o,0,Fo\right)=0 \ \text{ and } \ \left.\frac{\partial\theta}{\partial z}\right|_{\left(r_i\le r\le r_o,0,Fo\right)}=0 \\
u\left(r_i\le r\le r_o,L,Fo\right)=0,\ \ w\left(r_i\le r\le r_o,L,Fo\right)=0 \ \text{ and } \ \left.\frac{\partial\theta}{\partial z}\right|_{\left(r_i\le r\le r_o,L,Fo\right)}=0
\end{gathered} \tag{8}$$

Effective local and average Nusselt number as well as melting volume fraction defined on the left hot wall of inner pipe and all of the area between two pipes can be written, respectively:

$$\text{Nu}_{\text{local,eff}} = -\frac{k_{\text{eff}}}{k_{\text{bf}}}\frac{\partial\theta}{\partial r},\ \ \text{Nu}_{\text{avg,eff}} = \int_0^1 \text{Nu}_{\text{eff}}\,\text{d}z = -\frac{k_{\text{eff}}}{k_{bf}}\int_0^1 \frac{\partial\theta}{\partial r}\,\text{d}z,\ \ MVF = \frac{\int_A \phi(T)\,\text{d}A}{\int_A \text{d}A} \tag{9}$$

Numerical method

Governing equations of the problem, including the continuity, momentum, and the energy equations along with the boundary conditions, have been solved by the finite element method. In this study enthalpy porosity technique employed for the numerical solution of non-Newtonian PCM melting saturated in copper porous foam and clear zone. The continuum equation is used as a constraint to satisfy the mass conservation. Hence, this constraint is considered for the continuum equation as a penalty parameter, γ, in momentum equations. A grid independency test has been carried out in order to find the acceptable grid size which will provide exact sufficient answers with a logical computational cost. To check the grid independency of solution, regard to the calculations were repeated for five kinds of uniform quadrangle networks with sizes 2700, 5925, 10400, 23100, and 31325 for Pr = 50, Ra = $5 \cdot 10^3$, Ste = 0.02, $\varepsilon = 0.5$, and $n = 0.8$. The results for different grid sizes and melting volume fraction are show in tab. 2. The conclusions of tab. 2 depict that the grid size of 23100 can provide reasonable precision. Hence, the outcomes of the present research are accomplished using the mesh size 23100.

Table 2. Nusselt number and melting volume fraction of the hot wall for different uniform grids, Ra = 5000, n = 0.8, Da = 10^{-3}, Ste = 0.02 an d = 0.5

Number of element	Time	Percentage error of melting volume fraction [%]			Percentage error of Nusselt number [%]		
		Fo = 0.005	*Fo* = 0.005	*Fo* = 0.005	*Fo* = 0.005	*Fo* = 2	*Fo* = 5
2700	2 hours and 15 minutes	–	–	–	–	–	–
5925	4 hours and 43 minutes	1.98	0.14	0.29	20.94	2.35	3.68
10400	10 hours and 42 minutes	0.06	0.47	0.23	2.67	0.82	1.98
23100	47 hours and 16 minutes	0.07	0.41	0.25	7.49	0.53	0.63
31325	84 hours and 9 minutes	1.59	0.46	0.29	37.76	0	0.85

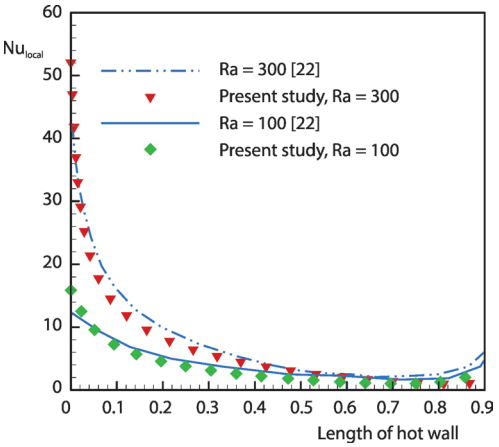

Figure 2. Comparison of the local Nusselt number obtained by Sheremet and Pops [22] with present work

Validation of computation

For the first case, fig. 2 depicted a comparison of the local Nusselt number obtained by Sherement and Pops [22] with current research in two Rayleigh numbers Ra = 100 and Ra = 300. They have studied, natural convection heat transfer of nanofluid in a triangular cavity filled with porous media. The vertical wall was considered at higher temperature and local Nusselt number evaluated on this wall. As can be seen in fig. 2, the results of the current study have good agreement with the results of Sherement and Pops [22] work. In the second case, a numerical model confirmation for horizontal shell and tube with the partial porous inserts was carried out by Xu *et al*. [23]. In that study a cross-section of two concentric tubes is considered. The porous inserts has a central angle of 30° of sector- ring shape with 0.8 porosity. The lithium carbonate and copper foam have been used as PCM and porous media. The inner tube is considered at higher temperature than the outer tube. Comparison have been done for the melting fraction of lithium carbonate at times of 100, 500, and 3500 seconds. It can be found from fig. 3 that there is a good compatibility between the conclusions of the present simulation and the outcomes of Xu *et al.* [23].

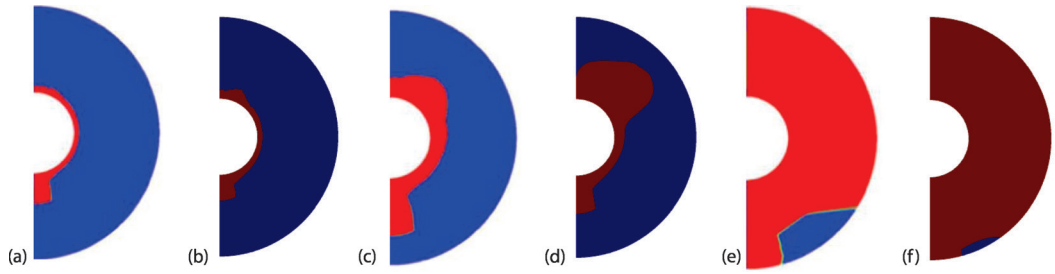

Figure 3. A comparison of the melting fraction in the full porous PCM (Case III) *vs*. results by [23]; (a) t = 100 s [23], (b) t = 100 s, present work, (c) t = 500 s [23], (d) t = 500 s, present work, (e) t = 3500 s [23] and (f) t = 3500 s, present work

Outcomes and discussion

Effect of Rayleigh number, porosity, Carreau index and Stefan number on the streamlines, isotherms, melting fraction and average Nusselt number have been demonstrated. It is worth to note that we have considered default values for different parameters and numbers as $n = 0.8$, $\varepsilon = 0.5$, Pr = 50, Da = 10^{-3}, Ra = 5000, and Ste = 0.02.

Impact of Rayleigh number on the melting process

Figure 4 illustrates the streamlines, isotherms, and melting fractions of PCM based on various Rayleigh numbers. As it is evident in the porous medium on the left half, the increase of Rayleigh number from 500-5000 is not causing any significant change in the patterns of mentioned results. Indeed, conduction heat transfer is the dominant mode in the porous medium. Hence, convection heat transfer mode has a neglect effect on the porous left side. However, in the right region, which is a clear medium, the dominant heat transfer mode is the natural convection type. Therefore, increasing in Rayleigh number significantly affects the streamlines, the isotherms and the melting volume fraction of PCM in the right half. It is important to note that by moving away from the porous medium the impact of the Rayleigh number increases. So that the difference between each one of the streamlines, isotherms, and the melting volume fraction patterns of PCM become the maximum value in vicinity of the right cold wall. It can be found

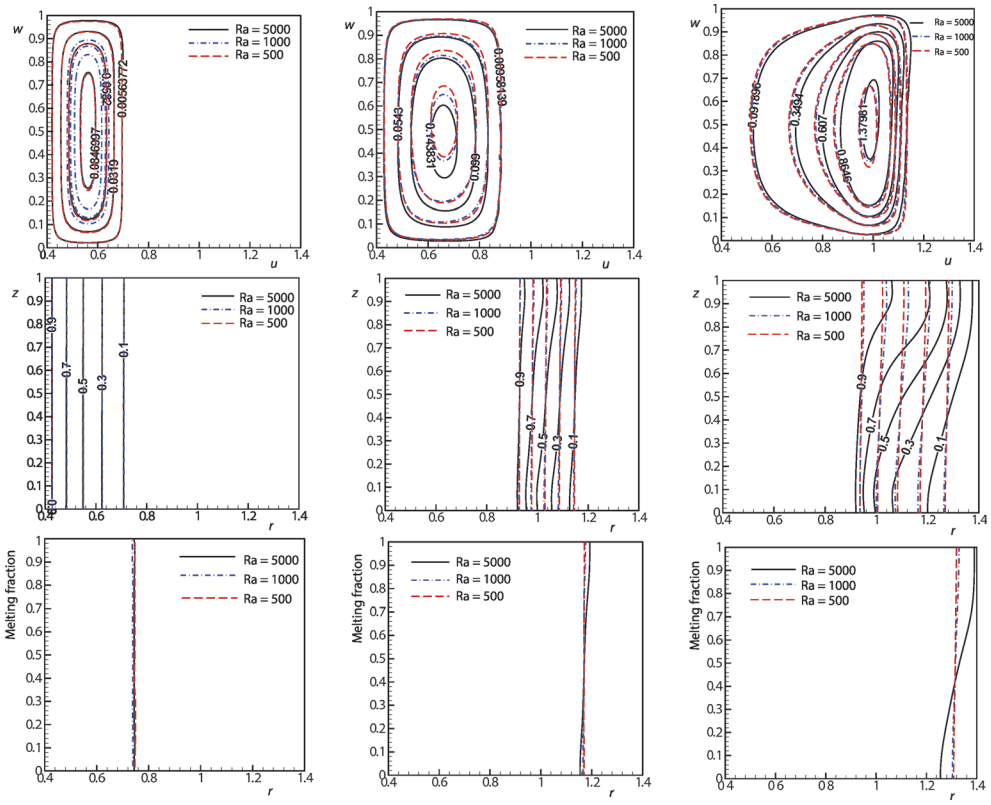

Figure 4. Evaluation of the streamlines, contour of isotherms and melting fraction for different Rayleigh numbers, Ra = 500, Ra = 1000, and Ra = 5000 in default values; (a) *Fo* = 0.002, (b) *Fo* = 2, and (c) *Fo* = 5

that increment in Rayleigh number in the clear right medium enhances convective mode, which improves the fluid velocity in the space between two pipes and augments the heat transfer and ultimately increases the melting rate of paraffin wax. Figure 5 demonstrates average Nusselt number and the melting volume fraction of PCM during the non-dimensional time of zero up to five based on different Rayleigh numbers. As seen the obtained pattern for average Nusselt number is completely opposite of the melting volume fraction pattern. It means that as time passes, average Nusselt number decreases while melting volume fraction of PCM increases. Indeed, the maximum value of average Nusselt number means the huge thermal gradients. In the early times, due to the high temperature difference between the solid PCM phase and the hot surface of inner pipe severe thermal gradients occurs near the inner pipe. By satisfying the melting condition, paraffin wax transforms into a mushy form then fluidic phase. Overtime, as the melting front spreads, phase change material and the hot surface of inner pipe tend to thermal equilibrium. Therefore, average Nusselt number decreases in vicinity of the hot wall during developing the melting volume fraction of paraffin wax.

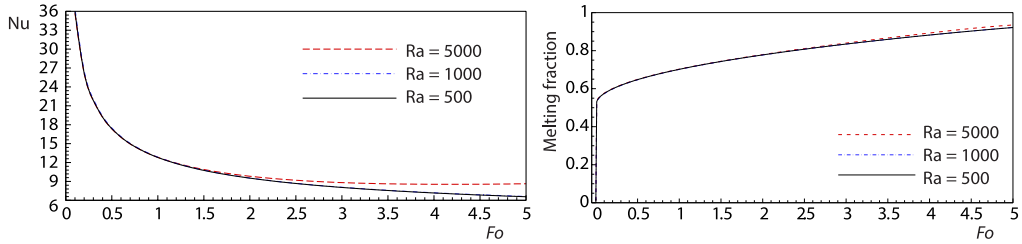

Figure 5. A comparison of Nusselt number and melting fraction for different Rayleigh numbers in default values

Impact of porosity index on the melting process

Figure 6 shows Nusselt number and the melting fraction of PCM as a function of non-dimensional time. Considering depicted results in fig. 6, in the early times for high values of porosity parameter, the region on the left half changes from porous to a clear medium. Decrease in the thermal gradients leads to deteriorate of average Nusselt number in vicinity of the hot surface of inner pipe. As time progresses and the PCM moves away from the hot surface, the value of thermal gradients formed for different values of porosity parameter are approximately equal. In the areas away from the hot surface, conductivity properties of solid matrix of porous medium has a very low effect on the PCM, hence the curves related to Nusselt number get closer as the time passes. Also, at a higher value for the porosity index ($\varepsilon = 0.8$), a more time is needed to melt the paraffin wax. The melting process of PCM in the porous media with the porosity parameter of 0.8 is slower and when the density of porous medium is high ($\varepsilon = 0.1$), the melting process becomes faster.

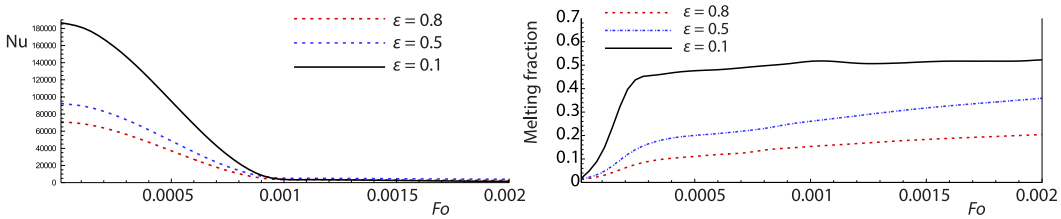

Figure 6. Average Nusselt number and melting volume fraction *vs.* non-dimensional time for different porosity index in default values

Impact of Carreau index on the melting process

Figure 7 shows the average Nusselt number and the PCM melting fraction, during non-dimensional time of zero up to 5 for different values of Carreau index. It can be seen, in the early times (the time that melting occurs in the porous medium), the patterns of the average Nusselt number and the PCM melting fraction are really close to each other. However, as the time passes and the melted paraffin wax progresses in the clear medium, the gap between the curves widens, so that in the last non-dimensional time (Fo = 5) this gap is at its maximum value. It is observed that the pseudo-plastic fluid has the highest heat transfer rate and melting volume fraction.

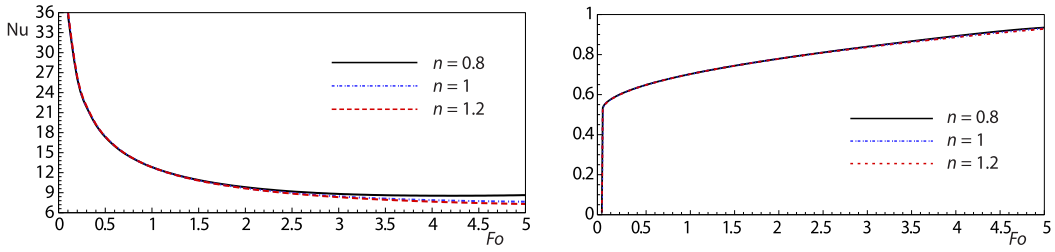

Figure 7. A comparison of Nusselt number and melting fraction for different values of Carreau index in default values

Impact of Stefan number on the melting process

Figure 8 demonstrates the effect of Stefan number on the heat transfer rate and melting volume fraction of PCM, respectively. The average Nusselt number for high Stefan numbers (Ste = 0.12) has lower values at predetermined times. In other words, when Stefan number increases, severe thermal gradients occur in the earlier times (less than $5 \cdot 10^{-3}$). Therefore, in the earliest time shown ($5 \cdot 10^{-3}$), for high values of Stefan number, the inner hot wall and the phase change material have moved to the thermal equilibrium. After a while and after thermal equilibrium stabilization in the three curves, it can be found the heat transfer is higher for high Stefan numbers. As the temperature of inner hot wall increases the heat transfer rate improves throughout the space. It also increases the PCM melting velocity. The melting fraction of PCM for high Stefan numbers has significant developments in early times. At the end (in Fo = 5), melting volume fraction of PCM with respect to high Stefan number would be more than those of low Stefan numbers and PCM melting process almost completes.

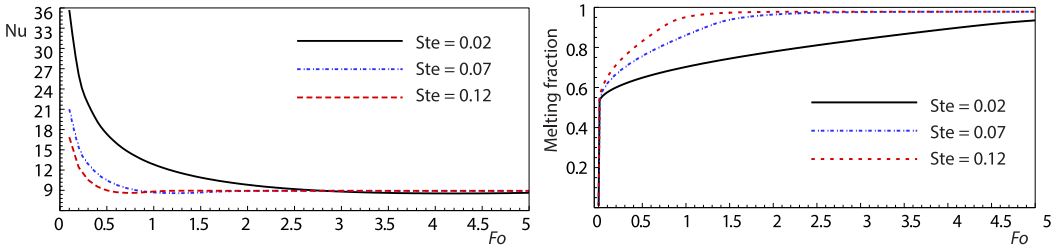

Figure 8. Average Nusselt number and melting fraction against non-dimensional time for different Stefan numbers in default values

Conclusions

Utilizing the enthalpy-porosity method, the PCM melting process of paraffin wax in the space between two concentric pipes was studied. The governing equations have been identified, transformed into their non-dimensional form, and solved through finite element method. The effects of various factors such as Rayleigh number, porosity parameters, Carreau index, and Stefan number on the streamlines, isotherms, melting volume fraction of PCM, and the average of Nusselt number have been evaluated. The prominent results are summarized as follows.

- Since the heat transfer mechanism is conduction mode in porous medium, the changes of Rayleigh number has not any significant effect on the streamlines, isotherms, and melting volume fraction of paraffin wax in the left half. Instead, in the clear medium on the right half side of considered space, increasing the Rayleigh number improves the development of melting fraction of PCM.
- Porosity parameter has significant impact on the streamlines, isotherms, and melting volume fraction of PCM only in the porous medium. Porous medium tends to a clear medium by increasing porosity parameter. Therefore, the reinforcement of the porosity parameter results in an extreme reduction in melting volume fraction of PCM and Nusselt number.
- Paraffin wax, as a non-Newtonian pseudo plastic fluid (shear thinning fluid) with Carreau index of $n < 1$, melts faster than Newtonian ($n = 1$) and non-Newtonian dilatant fluids. It is more significant in the non-porous right half.
- Stefan number has a clear effect in the space of between two pipes. This effect is stronger in the porous medium and moving away from this medium toward the clear medium the impression of Stefan number on the melting volume fraction of PCM becomes weak.

Nomenclature

A_m – Mushy-zone constant, [kgm^{-3}s^{-1}]
C – specific heat, [Jkg^{-1}K^{-1}]
C_p – specific heat in constant pressure, [Jkg^{-1}K^{-1}]
Da – Darcy number, [–]
g – gravity, [ms^{-2}]
K – permeability of porous foam, [m^{-2}]
k – thermal conductivity, [Js^{-1}m^{-2}K^{-1}]
L – latent heat of fusion, [Jkg^{-1}]
n – Carreau index, [–]
P – pressure, [Pa]
Pr – prandtl number, [–]
r – radius of the cylinder, [m]
Ra – Rayleigh number, [–]
Ste – Stefan number, [–]
$s(\theta)$ – Carman-Kozeny equation, [–]
T – temperature, [K]
T_f – melting temperature, [K]
t – time, [s]
u – velocity in the r- direction, [ms^{-1}]
w – velocity in the r-direction, [ms^{-1}]

Greek symbols

β – thermal expansion coefficient, [K^{-1}]
$\dot{\gamma}$ – shear rate, [s^{-1}]
ε_p – Carman- Kozeny equation constant, [–]
θ – non-dimensional temperature, [–]
λ – time dependent parameter, [s]
μ – dynamic viscosity, [kgm^{-1}s^{-1}]
ρ – density, [kgm^{-3}]
$\varphi(\theta)$ – liquid fraction, [–]

Subscripts

c – cold
f – fusion
h – hot

References

[1] Nomura, T., *et al*., Heat Storage in Direct-Contact Heat Exchanger with Phase Change Material, *Applied Thermal Engineering*, *50* (2013), 1, pp. 26-34
[2] Liu, Z., *et al*., Numerical Modelling for Solid-Liquid Phase Change Phenomena in Porous Media: Shell-and-Tube Type Latent Heat Thermal Energy Storage, *Applied Energy*, *112* (2013), Dec., pp. 1222-1232
[3] Chamkha, A. J., *et al*., Phase-Change Heat Transfer of Single/Hybrid Nanoparticles-Enhanced Phase-change Materials over a Heated Horizontal Cylinder Confined in a Square Cavity, *Advanced Powder Technology*, *28* (2017), 2, pp. 385-397

[4] Tian, Y., Zhao, C. Y., A Numerical Investigation of Heat Transfer in Phase Change Materials (PCM) Embedded in Porous Metals, *Energy*, *36* (2011), 9, pp. 5539-5546
[5] Adhikari, B., Jindal, V. K., Artificial Neural Networks: A New Tool for Prediction of Pressure Drop of Non-Newtonian Fluid Foods through Tubes, *Journal of Food Engineering*, *46* (2000), 1, pp. 43-51
[6] Poulikakos, D., Spatz, T. L., Non-Newtonian Natural-Convection at a Melting Front in a Permeable Solid Matrix, *International Communications in Heat and Mass Transfer*, *15* (1988), 5, pp. 593-603
[7] Kim, G. B., *et al*., Transient Buoyant Convection of a Power-Law Non-Newtonian Fluid in an Enclosure, *International Journal of Heat and Mass Transfer*, *46* (2003), 19, pp. 3605-3617
[8] Lamsaadi, M., *et al.*, Natural-Convection Heat Transfer in Shallow Horizontal Rectangular Enclosures Uniformly Heated from the Side and Filled with Non-Newtonian Power Law Fluids, *Energy Conversion and Management*, *47* (2006), 15-16, pp. 2535-2551
[9] Vinogradov, I., *et al*., Heat Transfer of Non-Newtonian Dilatant Power Law Fluids in Square and Rectangular Cavities, *Journal of Applied Fluid Mechanics*, *4* (2011), 3, pp. 37-42
[10] Turan, O., *et al*., Laminar Natural-Convection of Power-Law Fluids in a Square Enclosure with Differentially Heated Side Walls Subjected to Constant Temperatures, *Journal of Non-Newtonian Fluid Mechanics*, *166* (2011), 17-18, pp. 1049-1063
[11] Siavashi, M., Rostami, A., Two-Phase Simulation of Non-Newtonian Nanofluid Natural-Convection in a Circular Annulus Partially or Completely Filled with Porous Media, *International Journal of Mechanical Sciences*, *133* (2017), Nov., pp. 689-703
[12] Huang, C. J., Influence of non-Darcy and MHD on Free Convection of non-Newtonian Fluids over a Vertical Permeable Plate in a Porous Medium with Soret/Dufour Effects and Thermal Radiation, *International Journal of Thermal Sciences*, *130* (2018), Aug., pp. 256-263
[13] Kefayati, G. R., Simulation of Double Diffusive Natural-Convection and Entropy Generation of Power-Law Fluids in an Inclined Porous Cavity with Soret and Dufour Effects – Part II: Entropy Generation, *International Journal of Heat and Mass Transfer*, *94* (2016), C, pp. 582-624
[14] Chen, H. T., Chen, C. K., Natural-Convection of Non-Newtonian Fluids about a Horizontal Surface in a Porous Medium, *Journal Energy Resour. Technol*., *109* (1987), 3, pp. 119-123
[15] Hashim, A., Multiple Nature Analysis of Carreau Nanomaterial Flow Due to Shrinking Geometry with Heat Transfer, *Applied Nanoscience, 10* (2020), 8, pp. 3305-3314
[16] Sardar, H., *et al*., Mixed Convection Flow and Heat Transfer Mechanism for Non-Newtonian Carreau Nanofluids under the Effect of Infinite Shear Rate Viscosity, *Physica Scripta*, *95* (2020), 3, 035225
[17] Harab, B. A., *et al*., Numerical Investigation of Transient Natural-Convection Heat Transfer of Non-Newtonian Nanofluids between Eccentric Annulus, *Arabian Journal for Science and Engineering*, *44* (2019), 6, pp. 5631-5646
[18] Mehryan, S. A. M., *et al*., Melting Heat Transfer of Power-Law Non-Newtonian Phase-Change Nanoenhanced n-Octadecane-Mesoporous Silica ($MPSiO_2$), *International Journal of Heat and Mass Transfer*, *151* (2020), 6, pp. 5631-5646
[19] Ghalambaz, M., *et al*., Non-Newtonian Phase-Change Heat Transfer of Nanoenhanced Octadecane with Mesoporous Silica Particles in a Tilted Enclosure Using a Deformed Mesh Technique, *Applied Mathematical Modelling*, *85* (2020), Sept., pp. 318-337
[20] Khan, M., *et al*., Non-Linear Radiative Heat Transfer Analysis during the Flow of Carreau Nanofluid Due to Wedge-Geometry: A Revised Model, *International Journal of Heat and Mass Transfer*, *131* (2019), Dec., pp. 1022-1031
[21] Bird, R. B., *et al*., *Dynamics of Polymeric Liquids*, *Fluid Mechanics*, Willy, New York, USA, 1987, Vol. 1
[22] Sheremet, M. A., Pop, I., Free Convection in a Triangular Cavity Filled with a Porous Medium Saturated by a Nanofluid, *International Journal of Numerical Methods for Heat & Fluid-Flow*, *25* (2015), 5, pp. 1138-1161
[23] Xu, Y., *et al*., Melting Performance Enhancement of Phase Change Material by a Limited Amount of Metal Foam: Configurational Optimization and Economic Assessment, *Applied Energy*, *212* (2018), C, pp. 868-880

Paper submitted: July 11, 2020
Paper revised: October 2, 2020
Paper accepted: October 5, 2020